SUPPORTING INFORMATION

for

Mechanisms of physically irreversible fouling during surface water microfiltration and mitigation

by aluminum electroflotation pretreatment

Neranga P. Gamage[1] and Shankar Chellam[1, 2, *]

[1] Department of Civil and Environmental Engineering, University of Houston, TX 77204-4003

[2] Department of Chemical and Biomolecular Engineering, University of Houston, TX 77204-4004

*Correspondence to be sent to: chellam@uh.edu

Prepared for *Environmental Science and Technology*

Number of pages (including cover page): 13

Number of Tables: 7 (Table S1 and S7)
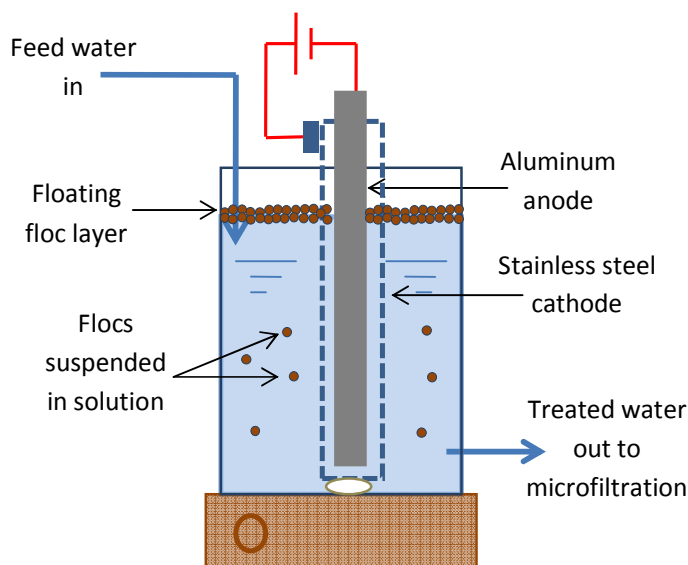
Number of Figures: 6 (Figure S1-S7)

Figure S1. Schematic of electroflotation cell used in the experiments.

Table S1. Calculation of % atomic concentration of elemental O foulants present on the membrane surfaces (pretreated and untreated) corresponding to cycle1, 3, and 5. Atomic concentrations were adjusted to minimize contributions from the virgin membrane[1]. Here, O concentration of the virgin membrane after multiplying by the F concentration ratio between fouled and virgin membrane surfaces (F/F_{virgin} where F_{virgin} = 28.80) was subtracted from that of the fouled membranes.

Cycle	$O_{foulant+membrane}$		$C_{foulant+membrane}$		F		F/F_{virgin}		$O_{foulant} = O_{foulant+membrane} - F/F_{virgin} \times O_{virgin}$		$C_{foulant} = C_{foulant+membrane} - F/F_{virgin} \times O_{virgin}$	
	Raw	EF	Raw	EF	Raw	EF	Raw	EF	Raw	EF	Raw	EF
1	16.66	19.97	54.85	51.93	26.83	25.36	0.93	0.88	3.05	7.12	2.14	2.10
3	19.57	24.56	52.19	47.81	23.60	22.09	0.82	0.77	7.60	13.37	5.82	4.41
5	21.36	26.54	50.36	45.36	21.49	20.39	0.75	0.71	10.47	16.20	8.15	5.29

Carbon, Fluorine and oxygen contents of the virgin membrane were 56.59%, 28.8% and 14.6% respectively.

One set of example calculations are presented next. Here, since oxygen was present in both the foulants and the virgin membrane, fluorine signal which was absent in the foulants was used to adjust the contribution of oxygen from the virgin membrane[1]. In the case of no pretreatment cycle 5 (raw), following steps were followed when adjusting O contribution from the virgin membrane.

1. Calculate the ratio between F concentrations on the fouled membrane and virgin membrane (F_{fouled}/F_{virgin} =21.49/28.80=0.75).

2. Multiply the calculated ratio by % atomic concentration of O on the virgin membrane (14.60) which is the contribution of O from the membrane itself (0.75x21.36=10.95).

3. Subtract the contribution of O from the membrane from the total O concentration measured from the fouled membrane (21.36) which is the O contribution from the foulants only (21.36-10.95=10.41) or "virgin membrane adjusted O concentration".

4. Divide the "virgin membrane adjusted O concentration" by the C concentration of the fouled membrane (50.36) which is the "virgin membrane adjusted O/C ratio" (10.41/50.36=0.2067).

Table S2. % atomic concentrations of N, Al, Si, O, and C detected on the irreversibly fouled membrane surfaces corresponding to pretreated and untreated cases for cycle1, 3, and 5. Since C and O had contributions from both the virgin membrane and from the foulants, their concentrations were adjusted to minimize the contribution from the virgin membrane (see Table S1).

Cycle	N		Al		Si		O		C	
	Raw	EF	Raw	EF	Raw	EF	Raw	EF	Raw	EF
1	0.14± 0.02	0.00	0.53± 0.08	2.57± 0.19	0.68± 0.06	0.00	2.83± 0.19	7.12± 0.23	2.31± 0.14	2.10± 0.13
3	0.80± 0.12	0.10± 0.03	0.71± 0.14	4.84± 0.08	2.48± 0.09	0.65± 0.15	7.60± 0.50	13.37± 0.57	6.15± 0.45	4.41± 0.13
5	1.65± 0.20	0.17± 0.03	0.87± 0.07	5.92± 0.18	3.51± 0.26	1.06± 0.03	10.13± 0.55	16.20± 0.04	8.81± 0.51	5.29± 0.33

Table S3. % atomic concentrations of source water, lake water after electroflotation (in floated floc layer, suspended flocs, and floated + suspended flocs), and "pure" coagulant formed by electrolyzing nanopure water. Concentrations corresponding to virgin membrane surface are also shown.

	C	N	Al	Si	O	F	Ca	Cl	Na	In
Source water	43.81	2.94	1.89	6.67	40.59	0.04	1.28	0.51	1.50	0.76
Electrofloated raw water — floated flocs	29.18	1.84	12.49	1.81	53.68		0.56			0.47
Electrofloated raw water — suspended flocs	36.48	2.15	10.41	4.21	46.05		0.11			0.54
Electrofloated raw water — floated + suspended flocs	32.83	1.995	11.45	3.01	49.36		0.34			0.51
"Pure" coagulant	9.47		21.48		67.69					1.35
Virgin membrane	56.59				14.60	28.80				

Table S4. Atomic concentration ratios of source water, lake water after electroflotation, "pure" coagulant formed by electrolyzing nanopure water, and virgin membrane surface.

	N/C	Al/O	Si/C	Al/C	O/C
Source water	0.07	0.05	0.15	0.04	0.92
Electrofloated raw water	0.06	0.23	0.09	0.36	1.52 (~1.06 from coagulant assuming Al:O=1:3)
"Pure "coagulant	0	0.32	0	2.25	7.15
Virgin membrane	0	0	0	0	0.26

Table S5. Organic and Al concentrations present in feed waters and amounts desorbed from the irreversibly fouled membranes using HCl (pH 2) and NaOH (pH 12) after cycle 1 and cycle 5 in the presence and absence of pretreatment.

Parameter	Untreated (Raw water)			Electrofloated		
	MF Feed concentration (mg/L)	Desorbed foulants - cycle 1 (mg/cm^2)	Desorbed foulants - cycle 5 (mg/cm^2)	MF Feed concentration (mg/L)	Desorbed foulants - cycle 1 (mg/cm^2)	Desorbed foulants - cycle 5 (mg/cm^2)
Al	0.21 ± 0.04	N/A	0.001± 0.001	3.10 ± 0.05	0.002 ± 0.001	0.010 ± 0.002

Al(OH)$_3$ (using Al:O=1:3)	N/A	N/A	0.003	~9.3	~0.006	~0.03
DOC	5.013 ± 0.4	0.011 ± 0.005	0.068 ± 0.01	3.031 ± 0.2	0.007 ± 0.003	0.038 ± 0.008
DOC + Al(OH)$_3$	N/A	~0.011	~0.071	N/A	~0.013	~0.068

Table S6. Peak assignments for FTIR spectra[2-9] (ν - stretching vibrations, δ - bending vibrations).

Peak Position (cm^{-1})	Peak Assignment
900-680	fingerprint region, ring breathing
695	N-H wagging
780, 798	Si-O-Si intertetrahedral bridging bond vibrations
850-680	νAl-O
798, 780	Si-O-Si intertetrahedral bridging bond vibrations
820-750	glycosidic linkages of polysaccharides
872	δC-H, δC-F
1100-950	Al-O-Al
1200-900	νC-O-C/ νC-O carbohydrates, ring vibrations
~1040	νC-O-C n-acetyl amino sugars in bacterial cell wall
1152	ν_{as}C-O-C, ring vibrations
1100	νSi-O amorphous (Si-O-Si)/biogenic silica (Si-O-C)
1184	νC-H, ν_sC-F
~1215	νC-C , νC-H , ν_{as}C-F
1280-1255	$\nu\phi$-OH (phenol), Amide III (νC=N + δN-H)
1280-1250	δC-OH of COOH and ϕ-OH
1314	δOH (primary, secondary), ν_{as}C-O-C (ester)
1340	δOH (tertiary, phenolic)
1500-1300	ν_sC(=O)O$^-$
1480-1400	νN-CH$_3$
1460-1378	δC-H
1510-1450	νC=C-C ring vibrations
1570-1545	Amide II ($\underline{\delta\text{N-H}}$ + νC-N)
1700-1500	ν_{as}C(=O)O$^-$
1650-1590	δOH of water
1620-1580	νC-C aromatic
1700-1600	Amide I ($\underline{\nu\text{C=O}}$ + δC-N + δN-H)
1755-1700	ν_{as}C(=O)OH, νC(=O)OR, νC=O (humics, lipids, fatty acids)
2750-2610	hydrogen bonded νOH of COOH
3000-2850	νC-H aliphatic
3050-3000	νC-H aromatic
3400-3050	νN-H from amino acids, proteins, and amino sugars
3750-3300	νO-H from carbohydrates, alcohols, Al-O-H, and Si-O-H

S1. Use of FTIR data to interpret interactions leading to membrane fouling

ATR-FTIR spectroscopy can be used in tandem with XPS analysis to identify foulants and to interpret interactions leading to physically irreversible fouling through changes in the prominent peaks of the functional groups responsible for, i) hydrogen bonding (frequency shifts towards lower wave numbers/ red

shifting of O-H/N-H band of IR spectrum at 3800-2500cm^{-1})[10], ii) complexation interactions (attenuation of C=O stretching vibration at ~1730-1720cm^{-1} and intensification of C(=O)O$^-$ stretching bands in the 1800-1300cm^{-1} region where the intensity of asymmetric vibration (1700-1550cm^{-1}) is greater than that of symmetric band (1500-1380cm^{-1}))[5, 11], and iii) hydrophobic interactions (intensity changes together with frequency shifts towards higher wave numbers/ blue shifting of C-H stretching bands in the 3050-2800cm^{-1} region which indicates the interactions of C-H groups with neighboring polar molecules providing indirect evidence for hydrophobic interactions)[12, 13].

Minor variations in the characteristic group vibrational frequencies arises as a result of local differences in molecular environment, either because of intra-molecular interaction between groups in the molecules, or intermolecular interaction with the surroundings[11]. These spectral changes can be used to investigate the interactions between a foulant moiety and its environment (e.g. virgin or foulant coated membrane). For example, weak interactions of foulant functional groups (e.g. O-H/N-H band, C-O-C band, amide I band) with Al(OH)$_3$ precipitates/ foulants/ membrane reduce their symmetry, activating vibrational modes which were otherwise inactive, hence leading to wider range of vibrational energies which broadens the IR peaks[11] of foulant sorbed flocs/ fouled membrane surface spectra compared with the spectrum of non-bonded sample (e.g. clean precipitates/ feed water/ virgin membrane). On the other hand, hydrogen bonding between O-H groups of foulants and membrane can stretch the O-H bond hence reducing its IR vibrational frequency compared to non-hydrogen bonded O-H groups (virgin membrane/ clean precipitates). This leads to red shifting of the OH/NH band which can be observed by its low frequency tail (i.e. greater intensity in the lower frequency side of the peak→3400-2500cm^{-1}) compared with non-hydrogen bonded virgin membrane or raw water spectra. Similarly, hydrogen bonding of C=O moiety of the peptide groups of proteins can stretch the C=O bond reducing its vibrational frequency. Hence red shifting of amide I band of fouled membrane spectrum compared with raw water spectrum indicates possible hydrogen bonding of C=O groups of proteinaceous foulants with the membrane surface. Cation mediated ligand exchange interactions (e.g. bridging) of carboxyl moieties of foulants with the carboxyl groups on the membrane surface lead to attenuation of C=O band of C(=O)OH groups due to deprotonation of the carboxyl groups and increase the intensity of symmetric and asymmetric carboxylate bands. Similarly,

electrovalent or electrostatic interactions of carboxylate groups also change the intensity of symmetric and asymmetric C(=O)O$^-$ bands.

Table S7 summarizes the spectral changes observed in this study in the regions associated with hydrogen bonding and hydrophobic interactions along with their interpretations (see Figure 2).

Table S7. List of IR spectral changes associated with hydrogen bonding and hydrophobic interactions of foulants with the membrane surface.

Spectrum	Vibration	Spectral change	(cm^{-1})	Interpretation
Figure 2: Raw water cycle 1	vC-H	Blue shift compared with virgin membrane	3022→3025, 2980→2984	Hydrophobic interactions/ interactions of C-H groups with polar moieties of virgin membrane
Figure 2: Raw water cycle 1	vO-H/N-H	Red shift compared with raw water	3750-2690→ 3720-2660	Hydrogen bonding between O-H groups of foulants and the virgin membrane
		Red shift compared with virgin membrane	3760-2720→ 3720-2660	
Figure 3: Raw water cycle 1	vC=O	Red shift compared with raw water	1654→1650 1640→1638	Hydrogen bonding of proteinaceous compounds with the virgin membrane
		Peak broadening compared with raw water	1565-1540→ 1580-1520	
Figure 2: Raw water cycle 5	vC-H	Blue shift compared with virgin membrane	3022→3025, 2980→2984	Hydrophobic interactions/ interactions of C-H groups with polar moieties of foulant coated membrane
Figure 2: Raw water cycle 5	vO-H/N-H	Red shift/greater intensity compared with raw water cycle 1	3720-2660→ 3700-2645	Greater extent of hydrogen bonding with successive cycling/ hydrogen bonding of foulants with the foulant coated membrane
Figure 2: Pretreated water cycle 1	vC-H	Blue shift compared with virgin membrane	3022→3025, 2980→2984	Hydrophobic interactions/ interactions of C-H groups with polar moieties of virgin membrane/coagulant
Figure 2: Pretreated water cycle 1	vO-H/N-H	Red shift compared with raw water	3750-2690→ 3680-2680	Hydrogen bonding of uncoagulated and coagulated foulants and Al(OH)$_3$ precipitates with the virgin membrane surface
		Red shift compared with virgin membrane	3760-2720→ 3680-2680	
Figure 2: Pretreated water cycle 5	vC-H	Blue shift compared with virgin membrane	3022→3025, 2980→2984	Interactions of virgin membrane C-H groups/C-H moieties of foulants with the surface hydroxyl groups of the coagulated flocs
Figure 2: Pretreated water cycle 5	vO-H/N-H	Greater red shift/ intensity compared with electrofloated water cycle 1	3680-2680→ 3660-2625	Hydrogen bonding of uncoagulated and coagulated foulants and Al(OH)$_3$ precipitates with the foulant coated membrane surface

S2. Particle size distributions. Compared to untreated Lake Houston water, % volume size distribution of the feed solutions after electroflotation shifted to right corresponding to greater particle sizes (Figure S2).

This shows that electroflotation increased the particle size of the colloids present in Lake Houston water (i.e. volume-based mean particle size: 23.28±3.18µm→73.96±7.11µm).
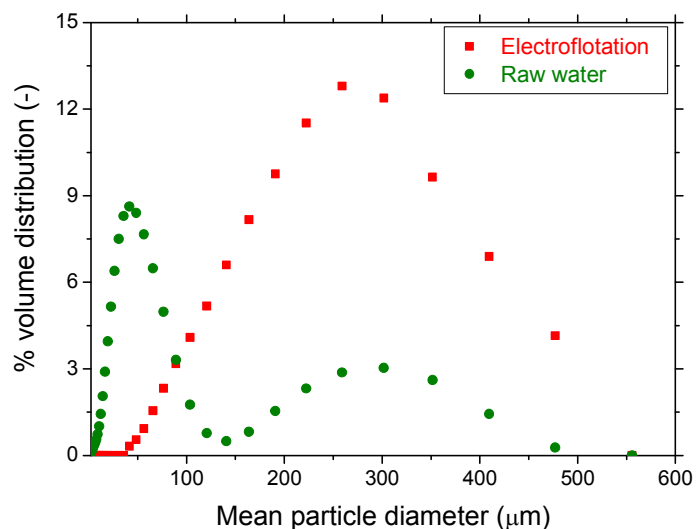

Figure S2. Particle size distributions of MF feed solutions in the presence and absence of electroflotation pretreatment.

S3. Composition of raw water contaminants. Raw water IR spectrum depicted in Figure S3 shows presence of protein-like, carbohydrate-like, humic-like, as well as siliceous compounds in Lake Houston water. The higher wavenumbers (3750-3300cm^{-1}) of the broad band centered around 3380cm^{-1} comprises of O-H stretching vibrations of alcohols and phenols whereas the lower wavenumbers (3400-3050cm^{-1}) correspond to N-H stretching of amines and amides as well as O-H stretching of carboxylic acids. This band also has contributions from Si-OH stretching vibrations as was confirmed by presence of Si-O-Si stretching vibrations at 780-800 and ~1100cm^{-1}, in tandem with the Si2p signal in XPS analysis. Symmetric (2850 and 2990cm^{-1}) and asymmetric (2916 and 3045cm^{-1}) alkyl and aromatic C-H stretching vibrations accompanied by C-C skeletal vibrations (1350-1000cm^{-1}) and C=C-C aromatic stretching vibrations (1615-1580 and 1510-1450cm^{-1}) are indicative of hydrocarbon backbone and aromatic rings of humic substances.
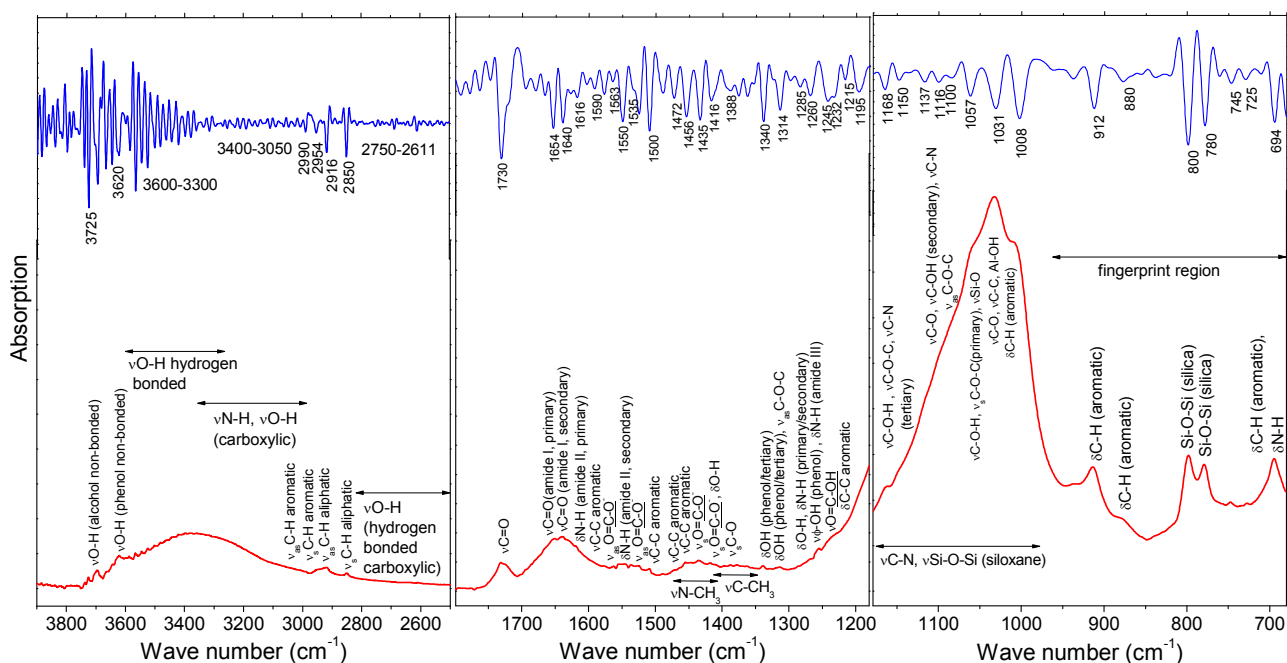
Figure S3. FTIR spectrum of source water with the second derivative spectrum showing the presence of carbohydrate-like, proteinaceous, humic-like and siliceous compounds of NOM.

The collective presence of amide peaks at 1700-1600, 1570-1545, 1300-1200, 3400-3050, and 725-670cm-1 arising from amide I, amide II, amide III, N-H stretching, and N-H wagging bands accompanied by N1s XPS signal (see SI) confirm the presence of proteinaceous foulants[3, 8]. Additionally, glycosidic (1200-1000cm-1) and N-CH3 (1480-1400cm-1) vibrations can be attributed to n-acetylamino sugars. Comparable results were reported by Lee at al. for isolated algal organic matter and surface water colloids[14]. Presence of carbohydrates were confirmed by the large broad peak at 1200-1000cm-1 (vC-OH: 1116, 1060cm-1, and vC-O-C: 1137, 1168, 1150cm-1) along with the -OH band at 3750-3300cm-1.

S4. *Increasing accumulation of foulants on the irreversibly fouled membrane surfaces.* Normalized FTIR spectra of membrane surfaces after cycles 1 and 5 are shown in Figure S2 for raw (solid blue cycle-5, dashed blue cycle-1) and electrofloated (solid red cycle-5, dashed red cycle-1) feed waters.

Band intensities corresponding to carbohydrate-like (vO-H 3750-3300cm^{-1}, vC-O-C/vC-O 1200-900cm^{-1}, vC-O-C 820-750cm^{-1}), proteinaceous (vN-H 3400-3050cm^{-1}, vC=O/vNH$_2$ 1650cm^{-1}, vN-H/vC-N 1540cm^{-1}, vC-O-C 1036cm^{-1}), humic-like (vC-H 3050-2800cm^{-1}, vC=C-C 1510-1450cm^{-1}, v(C=O)O$^-$ 1700-1300cm^{-1}), and siliceous (vSi-O-H 3750-3300cm^{-1}, vSi-O-Si 1100cm^{-1}, 800cm^{-1}, and 780cm^{-1}) increased from cycle-1 to cycle-5 . As seen in Figure S2, regions corresponding to O-H (3650-3200cm^{-1}) and Al-O (850-

680cm^{-1}) stretching vibrations significantly intensified even after cycle-1 both in the spectra corresponding to raw water and treated water suspensions. The intensity further increased for cycle-5 demonstrating progressive Al(OH)$_{3(s)}$ coagulant accumulation on pretreated-membrane surfaces.
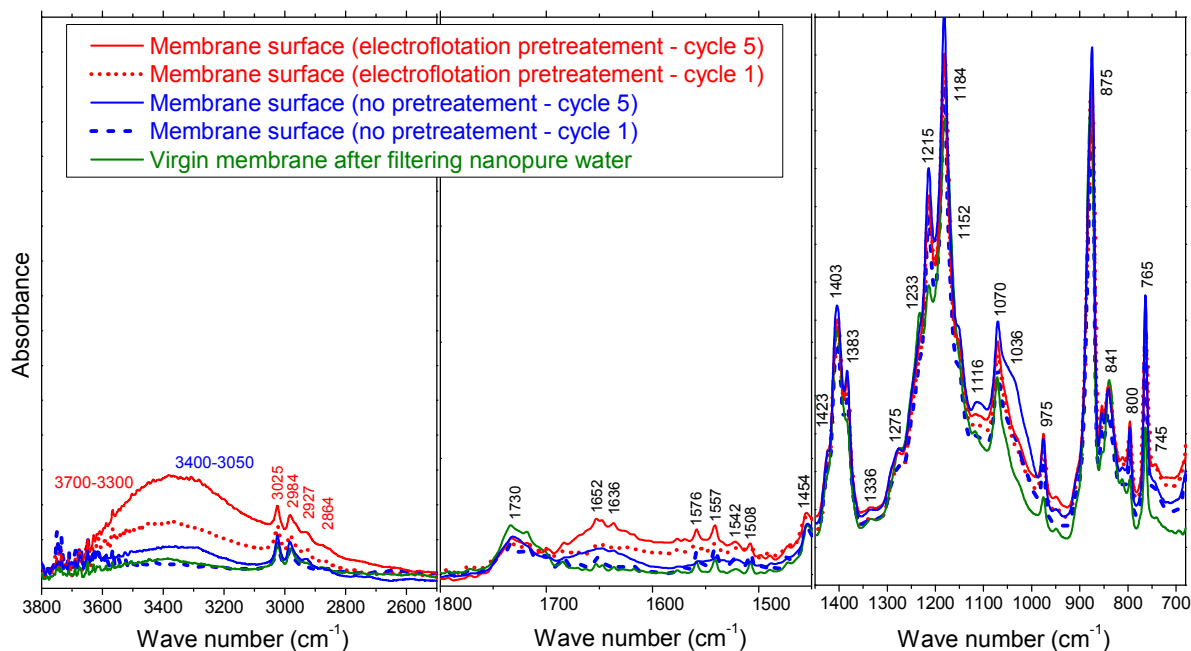

Figure S4. ATR-FTIR spectra of virgin membrane (green line), irreversibly fouled membrane surfaces operating on electrofloated water (solid red: cycle 5, dotted red: cycle 1), and untreated Lake Houston water (solid blue: cycle 5, dotted blue: cycle 1).

A magnified version of the IR spectra of raw water fouled membranes after cycles 1 and 5 as well as raw feed water spectrum in the symmetric and asymmetric stretching vibrations region is shown in Figure S5. The differences between the raw water fouled membranes' difference spectra and raw feed water spectrum is better visible in Figure S5 compared with Figure 3.
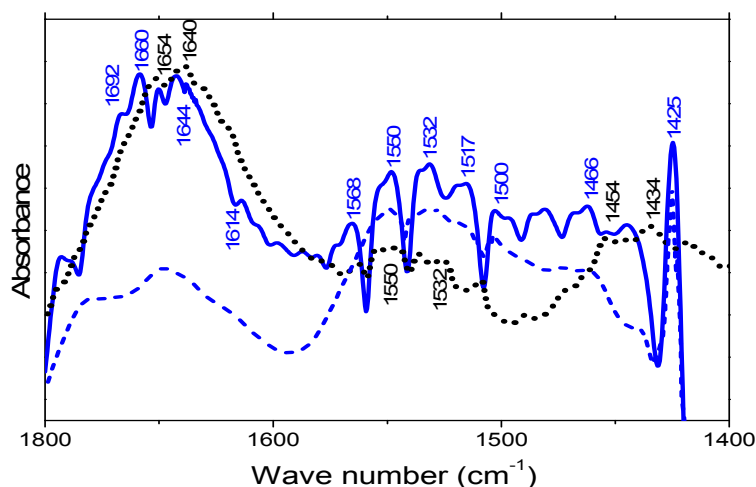

Figure S5. Symmetric and asymmetric stretching vibration region of carboxylate moieties corresponding to raw water - cycle 1, raw water - cycle 5, and raw water spectra of middle panel of Figure 3 magnified to better depict the spectral differences.

S5. XPS survey spectra of source water constituents, irreversibly fouled membrane and cake layer. XPS survey spectrum of raw water constituents revealed the presence of O, C, Al, Ca, Na, N, and Si (Figure S6a). Fe2p signal was absent in this spectrum due to its low concentration (0.07±0.03mg/L). As observed in Figure S6b, Ca was absent on the irreversibly fouled membrane surface even after the fifth filtration/regeneration cycle of source water filtration suggesting negligible complexation with the membrane. However, Ca2p signal was detected in the cake layer formed during forward filtration of Lake Houston water which was hydraulically removed during backwashing (Figure S6c) suggesting Ca^{2+} ions predominantly contributed to reversible fouling[15].
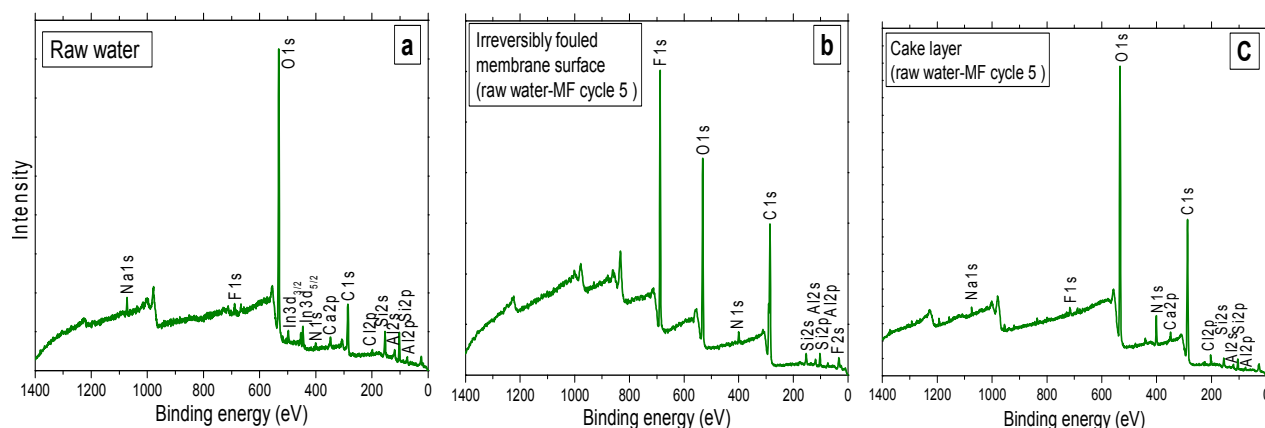

Figure S6. XPS survey spectra of (a) Lake Houston water, (b) membrane surface after source water filtration/regeneration cycle 5, and (c) cake layer after filtration of 150mL of Lake Houston water in the absence of pretreatment.

S6. Evidence for direct coagulant-membrane interactions. A control experiment was performed to investigate direct coagulant-membrane interactions leading to irreversible fouling, in the absence of other foulants present in natural water. In this experiment, nanopure water was electrolyzed to generate the same 10mg/L Al concentration used in electroflotation pretreatment of Lake Houston water. Next, the suspension consisting only of the "pure" coagulant was microfiltered and hydraulically regenerated prior to FTIR and XPS analysis. The top panel in Figure S7 depicts the IR spectrum of the "pure" coagulant precipitates generated in nanopure water (dotted green line) along with the difference spectrum of irreversibly fouled membrane after filtering this coagulant suspension (solid green line).

Emergence of new asymmetric (1580cm^{-1}) and symmetric (1470, 1438, 1418cm^{-1}) COO^{-} vibrations where greater relative intensity of asymmetric vibration in the spectrum corresponding to pure coagulant fouled membrane (solid green line) compared to unfiltered "pure coagulant" spectrum (dotted green line)

in the top panel of Figure S7 shows inner-sphere complexation between carboxylate groups on the membrane surface and the "pure" aluminum coagulant. Formation of more than one type of coordination complex was evidenced by the appearance of multiple symmetric and asymmetric bands. Their separation distances (Δv) varied between 110 and 170cm^{-1} indicating both chelating and bridging complexation of the coagulant with the membrane surface[5, 16, 17]. Clues to "Pure" coagulant – membrane inner-sphere complexation was also observed by O1s (middle panel in Figure S7) and C1s (bottom panel in Figure S7) core level analysis, which showed peak shifts and emergence of new peaks. These envelopes were fitted using the positions relative to the F1s peak of the membrane at 686.6eV (in virgin and fouled membrane spectra) and Al2p peak at 74.4eV (in "pure" coagulant spectrum). For example, O1s peaks in the irreversibly fouled membrane after filtration/regeneration of the coagulant in nanopure water showed that component peaks corresponding to the coagulant shifted to lower binding energies (O-I 530.7→530.4 and O-II 532→531.8eV), whereas that of membrane shifted to higher binding energies (C($\underline{=O}$)OH/C($\underline{=O}$)OR 531.4→531.8 and C-$\underline{O}$R/C-$\underline{O}$H 532.4→532.9eV). Moreover, an additional peak emerged between the coagulant peaks and membrane peaks at 531.7eV corresponding to the carboxylate groups inner-spherically complexed[18] with the virgin membrane surface. C1s spectra also provided evidence for inner-sphere complexation of carboxylic groups with the coagulant wherein the virgin membrane peak at 288.20eV has shifted to lower binding energies by 0.34eV (to 287.86eV) in the membrane surface fouled by the "pure" coagulant[19] (Bottom panel in Figure S7).
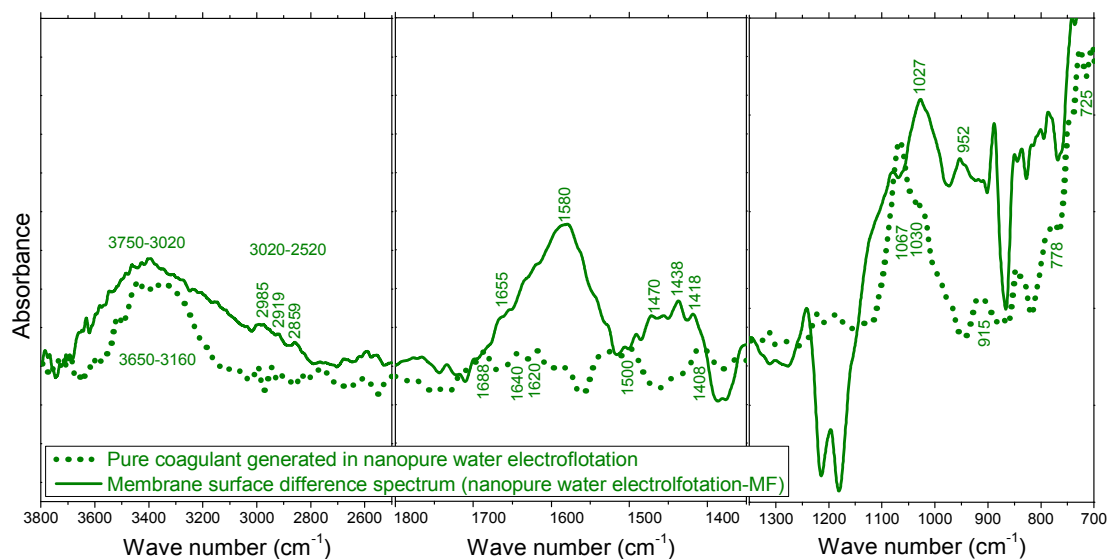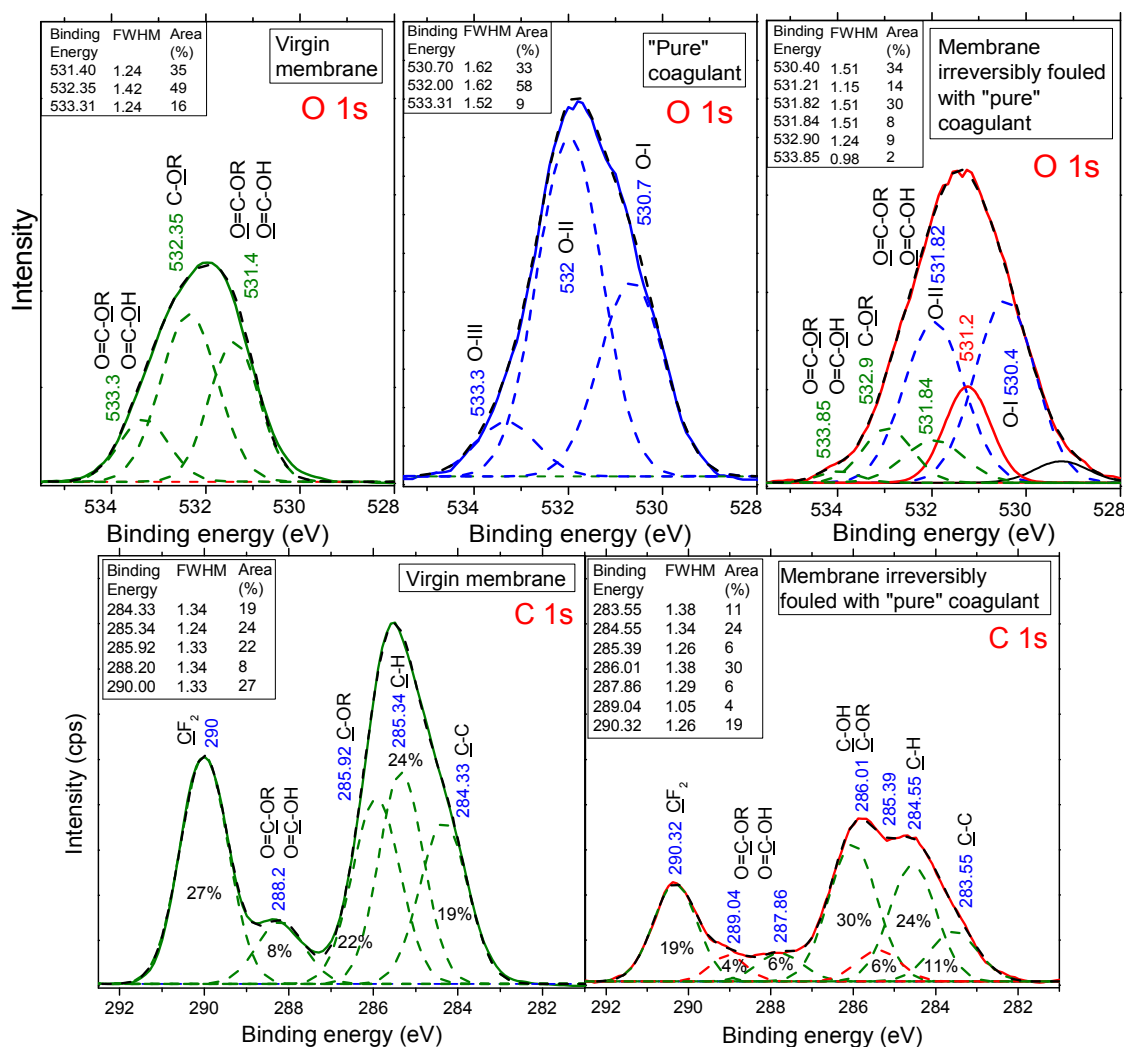
Figure S7. Spectra of coagulant and membrane in a control experiment. Top panel: ATR-FTIR difference spectra of coagulant in nanopure water and the membrane surface after filtering 100mL of the "pure" coagulant suspension and hydraulically regenerating it. **Middle panel:** XPS O1s core level spectra of virgin membrane, "pure" coagulant, and irreversibly fouled membrane following filtration of the "pure" coagulant suspension. **Bottom panel:** XPS C1s core level spectra of virgin membrane and irreversibly fouled membrane after filtration of the "pure" coagulant suspension.

REFERENCES

1. Riviáere, J. C.; Myhra, S., *Handbook of Surface and Interface Analysis : Methods for Problem-solving*. Marcel Dekker: New York, 1998.

2. Boccaccio, T.; Bottino, A.; Capannelli, G.; Piaggio, P., Characterization of PVDF membranes by vibrational spectroscopy. *Journal of Membrane Science* **2002**, *210*, (2), 315-329.

3. Lin-Vien, D., *The Handbook of infrared and raman characteristic frequencies of organic molecules.* Academic Press.: Boston, 1991.

4. Mantsch, H. H.; Chapman, D., *Infrared spectroscopy of biomolecules.* . Wiley-Liss.: New York, 1996.

5. Nakamoto, K., *Infrared and Raman Spectra of Inorganic and Coordination Compounds: Pt. B: Applications in Coordination, Organometallic, and Bioinorganic Chemistry*. Wiley Hoboken, NJ, 2009.

6. Nyquist, R. A., *Interpreting infrared, Raman, and nuclear magnetic resonance spectra.* Academic Press.: San Diego, 2001; Vol. 1.

7. Nyquist, R. A., *Interpreting infrared, Raman, and nuclear magnetic resonance spectra.* Academic Press.: San Diego, 2001; Vol. 2.

8. Stuart, B., *Infrared Spectroscopy: Fundamentals and Applications*. Wiley: Hoboken, NJ, USA, 2004.

9. Chen, J.; Gu, B.; LeBoeuf, E. J.; Pan, H.; Dai, S., Spectroscopic characterization of the structural and functional properties of natural organic matter fractions. *Chemosphere* **2002,** *48*, (1), 59-68.

10. Grabowski, S. J., *Hydrogen bonding - New insights*. Springer: Netherlands, 2006.

11. Little, L. H., *Infrared spectra of adsorbed species*. Academic Press: London, New York, 1966; p xii, 428 p.

12. Tanford, C., *The hydrophobic effect: formation of micelles and biological membranes*. 2 ed.; Krieger: Malabar, Fla, 1991.

13. Schmidt, P.; Dybal, J.; Trchová, M., Investigations of the hydrophobic and hydrophilic interactions in polymer–water systems by ATR FTIR and Raman spectroscopy. *Vibrational Spectroscopy* **2006,** *42*, (2), 278-283.

14. Lee, N.; Amy, G.; Croué, J.-P., Low-pressure membrane (MF/UF) fouling associated with allochthonous versus autochthonous natural organic matter. *Water Research* **2006,** *40*, (12), 2357-2368.

15. Ahn, W.-Y.; Kalinichev, A. G.; Clark, M. M., Effects of background cations on the fouling of polyethersulfone membranes by natural organic matter: Experimental and molecular modeling study. *Journal of Membrane Science* **2008,** *309*, (1–2), 128-140.

16. Gao, X.; Metge, D. W.; Ray, C.; Harvey, R. W.; Chorover, J., Surface Complexation of Carboxylate Adheres *Cryptosporidium parvum* Öocysts to the Hematite–Water Interface. *Environmental Science & Technology* **2009,** *43*, (19), 7423-7429.

17. Kang, S.; Xing, B., Adsorption of Dicarboxylic Acids by Clay Minerals as Examined by in Situ ATR-FTIR and ex Situ DRIFT. *Langmuir* **2007,** *23*, (13), 7024-7031.

18. Alexander, M. R.; Beamson, G.; Blomfield, C. J.; Leggett, G.; Duc, T. M., Interaction of carboxylic acids with the oxyhydroxide surface of aluminium: poly(acrylic acid), acetic acid and propionic acid on pseudoboehmite. *Journal of Electron Spectroscopy and Related Phenomena* **2001,** *121*, (1-3), 19-32.

19. Guan, X.-h.; Chen, G.-h.; Shang, C., ATR-FTIR and XPS study on the structure of complexes formed upon the adsorption of simple organic acids on aluminum hydroxide. *Journal of Environmental Sciences* **2007,** *19*, (4), 438-443.